

Flow Loop Experiments Using Polyalphaolefin Nanofluids

Ian C. Nelson* and Debjyoti Banerjee†

Texas A&M University, College Station, Texas 77843-3123

and

Rengasamy Ponnappan‡

U.S. Air Force Research Laboratory, Wright–Patterson Air Force Base, Ohio 45433-7251

DOI: 10.2514/1.31033

Experiments were performed using a flow-loop apparatus to explore the performance of nanofluids in cooling applications. The experiments were performed using exfoliated graphite nanoparticle fibers suspended in polyalphaolefin at mass concentrations of 0.6 and 0.3%. The experimental setup consisted of a test section containing a plain offset fin cooler apparatus (gap or nongap fin), which was connected to a flow loop consisting of a gear pump, a shell and tube heat exchanger (that was cooled or heated by a constant temperature bath chiller/heater), and a reservoir. Experiments were conducted using nanofluid and polyalphaolefin for two different fin strip layouts. Heat transfer data were obtained by parametrically varying the operating conditions (heat flux and flow rates). The heat transfer data for nanofluids were compared with the heat transfer data for neat polyalphaolefin fluid under similar conditions. The change in surface morphology of the fins was investigated using scanning electron microscopy. The nanofluid properties were measured using rheometry for the viscosity, differential scanning calorimetry for the specific heat, and laser flash apparatus for the thermal diffusivity. It was observed that the viscosity was ~10 times higher for nanofluids compared with polyalphaolefin and increased with temperature (in contrast, the viscosity of polyalphaolefin decreased with temperature). The specific heat of nanofluids was found to be 50% higher for nanofluids compared with polyalphaolefin and increased with temperature. The thermal diffusivity was found to be 4 times higher for nanofluids compared with polyalphaolefin and increased with temperature. It was found that, in general, the convective heat transfer was enhanced by ~10% using nanofluids compared with using polyalphaolefin. Scanning electron microscopy measurements show that the nanofluids deposit nanoparticles on the surface, which act as enhanced heat transfer surfaces (nanofins).

Nomenclature

A	=	area
A_c	=	area of cross section
A_h	=	heating area
C_p	=	specific heat capacity
D	=	hydraulic diameter
h	=	heat transfer coefficient
k	=	thermal conductivity
k_{fin}	=	thermal conductivity of fin material
L	=	length of pipe or tube
l	=	liquid property
l_1	=	length of fin
m	=	mean value
Nu	=	Nusselt number
n	=	number of fins
nf	=	properties of nanofluid
n_f, n_{st}	=	number of fins in each row and column
P	=	perimeter
Pe	=	Peclet number
Pr	=	Prandtl number
Q, q	=	total heat transfer rate, heat flux

Re	=	Reynolds number
s	=	fin parameter, surface property
T	=	temperature
U	=	mass averaged velocity
α	=	thermal diffusivity
κ	=	thermal conductivity
μ	=	viscosity
ρ	=	density
ϕ	=	volume fraction
Ω	=	forced convective heat transfer parameter

I. Introduction

NANOFUIDS are colloidal solvents containing dispersed nanometer (~10–100 nm) sized particles [1]. Nanofluids have been discovered to enhance the conductivity of solvents at low concentrations (<4%) as the size of the particles is decreased [2]. Large variations in thermal conductivity have been reported in the literature for various nanofluid compositions, that is, solvent type, pH of aqueous solvents, stabilizers (e.g., surfactants), material of the nanoparticles, concentration of the nanoparticles, size, and aspect ratio of the nanoparticles [3]. The enhancements in the thermal conductivity of the nanofluids were found to be higher than predicted by the classical theories [4,5]. These theories were proposed for heterogeneous colloidal mixtures of micron-scale particles in solvents. Several mechanisms have been proposed to account for the aberrant (or anomalous) behavior of the thermal conductivity of nanofluids [2,3].

A review of the recent literature and of the recently proposed theories suggests that localized Brownian convection is potentially the dominant mechanism responsible for the observed increase in thermal conductivity [6]. A comprehensive examination of the literature for aqueous nanofluids also shows a potential trend for maxima in the thermal conductivity of 10–50 nm diameter spherical nanoparticles [6,7]. This maxima is primarily governed by the competing effects of two transport resistances: 1) convective–conductive resistance arising from Brownian convection [6], and

Received 14 March 2007; revision received 8 September 2007; accepted for publication 14 October 2007. Copyright © 2008 by the American Institute of Aeronautics and Astronautics, Inc. The U.S. Government has a royalty-free license to exercise all rights under the copyright claimed herein for Governmental purposes. All other rights are reserved by the copyright owner. Copies of this paper may be made for personal or internal use, on condition that the copier pay the \$10.00 per-copy fee to the Copyright Clearance Center, Inc., 222 Rosewood Drive, Danvers, MA 01923; include the code 0887-8722/09 \$10.00 in correspondence with the CCC.

*Graduate Student, Department of Mechanical Engineering, Mail Stop 3123, Student Member AIAA.

†Assistant Professor, Department of Mechanical Engineering, Mail Stop 3123; dbanerjee@tamu.edu. Member AIAA.

‡Propulsion Directorate, Power Division, 1950 Fifth Street, Building B18, Associate Fellow AIAA.

2) liquid–solid interfacial resistance [7] on the surface of the nanoparticles. The former resistance dominates for the bigger particles (>10 nm), whereas the latter resistance dominates for the smaller particles (<10 nm). The competing resistances at different size ranges help to explain the maxima in the thermal conductivity observed in nanofluids. Incidentally, recent reports [7] contradict the previous thermal conductivity measurements and show that no enhancement of thermal conductivity was observed for nanoparticle diameters smaller than 10 nm. The potential reason for this lack of enhancement is that for such small nanoparticles the larger interfacial resistance masks any enhancement obtained from the localized Brownian convection.

Conductivity measurements could also be affected by the surface coating of the measurement probes caused by the precipitation of nanoparticles. Historically, measurements for the thermal conductivity of nanofluids reported in the literature [2,3] were based on the transient hot-wire (THW) method. However, THW is susceptible to measurement errors induced by the surface precipitation of nanoparticle suspensions, which the previous investigators have largely ignored in their studies. Hence, the proper design of experiments is needed to account for the effect of the surface precipitation of nanoparticles on the thermal conductivity measurements of nanofluids.

Nanofluids were also reported to enhance single-phase (forced convection and natural convection) as well as two-phase (pool boiling) convective heat transfer [2,6]. The critical heat flux (CHF) was reported to increase by 300% during pool boiling of nanofluids and the required wall superheat for a given heat flux was also found to increase for nanofluids compared with the pure solvent [8,9]. There are contradicting reports in the literature because a reduction in the pool boiling heat transfer coefficient was also reported for nanofluids [10–12]. The observed enhancement is possibly due to an increase in the number of nucleation sites, the size of the nucleation cavities, and the associated nucleation site density arising from the precipitation of the nanoparticles. Nanofluids are also known to have different wetting behavior [13]. In contrast, the enhanced fouling of the heater surface due to the rapid precipitation of the nanoparticles could also cause degradation of the pool boiling performance.

A systematic study on the effect of surface precipitation of nanoparticles on pool boiling is currently lacking in the literature. A recent study Guinn and Banerjee [14] reported that during spray boiling of nanofluids significant fouling of the heater surface occurred due to the precipitation of nanoparticles and this was observed to degrade the boiling heat transfer. Preliminary results from a recent study show that the surface precipitation of nanoparticles on a horizontal heater does change the surface characteristics and could be a dominant cause for change in pool boiling characteristics of nanofluids [15]. After the experimental runs, scanning electron micrography (SEM) images and energy dispersive x-ray (EDX) analysis showed that the gold nanoparticles were deposited on the heater surface from the nanofluids during boiling.

Although limited precipitation of nanoparticles can enhance the boiling heat transfer by increasing the nucleation site density and changing the wettability of the nanofluid on the heater surface, in single-phase flows such precipitations can enhance heat transfer by forming enhanced heat transfer surfaces (nanofins). Liquid thermal conductivity is ~ 100 – 1000 times smaller compared with solid materials [16]. Hence, seeding liquids with solid particles for enhancing the effective liquid conductivity has been subject of scientific interest for more than a century [4]. However, for evaluating the convective heat transfer enhancement in addition to the thermal conductivity, other thermophysical properties, such as thermal diffusivity, specific heat, and dynamic viscosity, as well as flow conditions, such as surface roughness and Reynolds number, are important factors that should be accounted for or measured experimentally. A review of the literature [2,3] for forced convection using nanofluids suggests that heat transfer was consistently increased by 8–15% for the same Reynolds number. Thus, there is less variability in the forced convective heat transfer data of nanofluids compared with the data for thermal conductivity or pool boiling [2,3]. However, it was found that the majority of these results

were reported using “effective” thermophysical properties of the nanofluids rather than experimental measurements for these properties (e.g., the volume expansion coefficient for natural convection experiments, as well as the specific heat, thermal conductivity, and viscosity for forced convection experiments). Also, the surface roughness of the heater surfaces was characterized before and after the experiments were performed using the nanofluids in only a limited number of studies.

Pak and Cho [17] used γ - Al_2O_3 and TiO_2 nanofluids in water where the particle sizes were 13 and 27 nm, respectively, for studying convective heat transfer in a pipe with an internal diameter of 1.07 cm and a length of 480 cm. The viscosity values for these nanofluids were found to be 200 times higher for γ - Al_2O_3 and 3 times higher for TiO_2 (than for water) at a 10% volume concentration each. The Reynolds number (Re) and Prandtl number (Pr) were varied from 10^4 to 10^5 and 6.5 to 12.3, respectively, in these experiments. The specific heat and thermal conductivity were estimated using empirical formulas and were not measured in these studies. The Darcy friction factor for nanofluids (volume fractions less than 3%) was measured to be within 3% of that for water for the same Reynolds number. This result is similar to the friction factor for 100 nm copper nanofluids in water where the friction factor was measured to be the same as for water at the same Reynolds number [18]. However, due to the significant increase in viscosity, comparisons for the same average velocity of the fluids showed that the pressure drop in nanofluids (2.78% γ - Al_2O_3) was 28% higher, the pumping penalty was 31% higher, and the friction factor was 36% higher than for water. In retrospect, the authors of this study probably could have obtained better results at a lower volume concentration of the nanoparticles. Based on the heat flux data, the authors proposed a new correlation for the turbulent flow of nanofluids:

$$Nu = 0.021Re^{0.8}Pr^{0.5} \quad (1)$$

In a subsequent study, CuO nanoparticles in water at a 0.9% volume concentration were found to augment the forced convection heat transfer coefficient by more than 15% [19]. Copper nanoparticles with a size less than 100 nm and a volume fraction of up to 2% were suspended in water and their convection properties were studied by Xuan and Li [18] for flow inside a 10-mm-diam brass tube, 800 mm long. The friction factors were found to be identical to that of water for Reynolds numbers in the range of 10,000–25,000. The Nusselt number variation of the nanofluids was found to be significantly underpredicted by the Dittus Boelter correlation [16]. The authors did not measure the associated thermofluidic properties but used an estimated value by using the effective thermal conductivity, diffusivity, and viscosity of the nanofluid. The Nusselt number of the nanofluids was found to be enhanced by up to 60% than that of water for the same Reynolds number and at a 2% volume concentration of the nanoparticles. Based on these measurements, the authors proposed a correlation for the convective heat transfer of the nanofluids:

$$Nu = c_1(1.0 + c_2\phi^{m_1}Pe_d^{m_2})Re_{nf}^{m_3}Pr_{nf}^{0.40} \quad (2)$$

where the subscript nf denotes effective nanofluid properties, ϕ is the volume fraction, Pe is the Peclet number [16] based on the diameter of the nanoparticle, and the constants for the correlation are denoted by c_1 , c_2 , m_1 , m_2 , and m_3 . At low volume fractions of the nanoparticles the pressure drop was found to be identical to that of water, and the authors did not find any pressure penalty associated with the nanofluids.

The heat transfer was enhanced locally by up to 47% for γ - Al_2O_3 /water nanofluid (~ 27 – 56 nm size nanoparticles, volume fractions up to 2%) in the entrance region of a 4.5-mm-diam tube, 970 mm long. The local enhancement was found to decrease with the axial distance from the entrance [20]. The authors proposed that the enhancement was due to particle migration that resulted in nonuniform distribution of thermal conductivity and viscosity as well as due to the reduced thickness of the thermal boundary layer. Such transient disruptions in viscosity, thermal conductivity, and

boundary-layer profile can also be expected due to the precipitation of nanoparticles on the tube walls. The effective viscosity was estimated using empirical equations, and the thermal conductivity was measured. The effective values of specific heat and density for the nanofluids were also estimated empirically in this study [21].

The laminar forced convection heat transfer was enhanced using Al_2O_3 /water (~ 20 nm particle size) and CuO /water (~ 50 – 60 nm particle size) nanofluids with volume fractions of 0.2–3% under constant temperature conditions [22]. The constant temperature condition was achieved by circulating steam in an outer jacket on a copper pipe with a diameter of 6 mm and a length of 1 m. The viscosity of the nanofluids was measured using a rheometer. The effective density, specific heat, and thermal conductivity were estimated from empirical equations in this study. The heat transfer coefficient was found to be enhanced by up to 40% compared with the theoretically predicted values for a given Peclet number. The enhancement was found to increase with particle concentration. A higher enhancement was observed for Al_2O_3 than for CuO .

The laminar forced convection heat transfer was enhanced using $\gamma\text{-Al}_2\text{O}_3$ /water (~ 20 nm particle size) nanofluids with volume fractions of 0.5, 0.75, and 1% under constant wall heat flux conditions [23]. The experimental apparatus consisted of a tube with a diameter of 1.02 mm and a length of 20 cm, and the flow rate was varied to achieve a maximum Reynolds number of 270. The heat transfer coefficient was found to decrease with the axial length until fully developed conditions were reached. The entrance length was found to agree with the analytical formulations in the literature. The heat transfer enhancement was found to depend on the Reynolds number and particle volume fraction. At a Reynolds number of 270, the heat transfer coefficient was enhanced by 8% for a volume fraction of 1% and by only 3% for a volume fraction of 0.5%. The authors attributed the enhancement to the Brownian convection of the nanoparticles and the interaction of the nanoparticles with the molecules of the base fluid as well as potentially to the formation clusters of the nanoparticles.

Interesting results were reported on the effect of the nanoparticle aspect ratio on the performance of the nanofluids for forced convective heat transfer augmentation [21,24]. The previous study [21] explored the effect of flow Reynolds number, temperature, nanoparticle loading, nanoparticle source, and the choice of base fluid on the heat transfer enhancement. Graphite nanoparticles with a 20–40 nm thickness and 1–2 μ in diameter (length to diameter: aspect ratio ~ 0.02) were suspended in two types of base fluids at concentrations of 2 and 2.5% by weight [24]. The first base fluid was a commercial-grade automatic transmission fluid (ATF) whereas the second base fluid was a mixture of synthetic base oils with commercial additive packages. The relevant liquid thermophysical properties were measured experimentally (e.g., density, viscosity, specific heat, and thermal conductivity) for the base fluids and the nanofluids. The thermal conductivity was found to be enhanced by 56%. The density and specific heat were not found to show much change. Depending on the concentration, the base fluids and nanofluids concentration, the viscosity was found to be enhanced by as much as 10% or was found to be reduced by up to 12%. The viscosity for both the base fluids and nanofluids was found to decrease with temperature. The nanofluids were tested in a flow-loop heat transfer apparatus (4.57-mm-diam pipe, 45.7 cm long) and the flow rates were varied 62–507 cm^3/min , which corresponded to average velocities of 6.3–52 cm/s as well as Reynolds numbers of 5–110. The heat transfer coefficient was enhanced by 22% for a 2.5% weight concentration at 50°C and by 15% at 70°C. The data were normalized on the basis of the Sieder–Tate correlation [25].

The objective of this study was to study the heat transfer enhancement in nanofluids (compared with the base fluid) from a plain array fin cooler. The motivation of the study was to produce preliminary data for exploring the applicability of nanofluids to various U.S. Air Force (USAF) thermal management applications, such as liquid-to-air heat exchangers, all electric aircraft technologies, directed energy weapon power thermal management (PTM), and aircraft PTM. The expected thermal enhancements could enable the reduction of aircraft components' size and weight. Other benefits include the

development of the technical know-how and capability to produce engineered (customized) coolants for retrofitting in future USAF air platforms. Exfoliated graphite (EG) nanoparticles suspended in polyalphaolefin (PAO) were used as the nanofluid for concentrations of 0.3 and 0.6% by weight with a particle diameter of 20 μ and a thickness of 100 nm. The thermal diffusivity, density, specific heat, and viscosity of the nanofluid were measured in the experiments. The surfaces of the plain fins were characterized before and after the experiments using SEM. The elemental chemical compositions of the deposited particles were characterized using EDX spectra. The deposited nanoparticles are believed to act as enhanced heat transfer surfaces (nanofins).

II. Experimental Apparatus and Procedure

A flow-loop experimental setup was used in this study. The experimental setup was originally designed for the measurement of the heat transfer and pressure drop in plain fin array coolers [26,27]. A schematic of the experimental setup is shown in Fig. 1. The experimental setup consists of a reservoir that connects to a flow meter. During initial experiment runs, a turbine type flow meter (with a signal conditioner) was used for measuring the flow rate of PAO. Because of the higher viscosity of the nanofluid, the turbine flow meter was found to be unsuitable for measurement. Hence, a positive displacement flow meter for high viscosity fluids was used (Omega model FPD1004-D-R-A with a display and reed switch and an output of 4–20 mA). Magnetically coupled gear pumps were used to pump the test fluid at flow rates up to 1.25 gal/min (0.079 L/s). The test fluid passed through a heat exchanger apparatus before entering the test section (cooling chamber) to obtain a constant inlet temperature for the cooler apparatus. The cooler apparatus housed a copper heat focusing block. Seven cartridge heaters and eight thermocouples were embedded in the heat focusing block. The heater apparatus was connected to a dc power supply and was used to heat the coolant in the cooler apparatus. The thermocouples were placed in the upper part of the heat focusing block and were arranged in four pairs in two horizontal planes. These thermocouples were used to measure the heat flux into the cooler at different locations (marked as E, W, N, S). The distance between each pair of thermocouples was 5.1 mm. The heater and cooler were insulated with fiberfax. Figure 2 shows a photograph of the experimental apparatus.

An array of plain fins was attached to the heater block (Fig. 3). The plain fins were available for different configurations, for example, offset, aligned, gap, and nongap. Offset gap fins were chosen for this study because, in previous studies, this configuration was observed to have the best cooling capability [26,27]. The fin array contained 14 rows of 20 copper fins and was soldered onto a substrate.

An intermediate plate (with a thickness of 0.8 mm) was mounted between the heater and fin array in the cooler. Machined slots in the

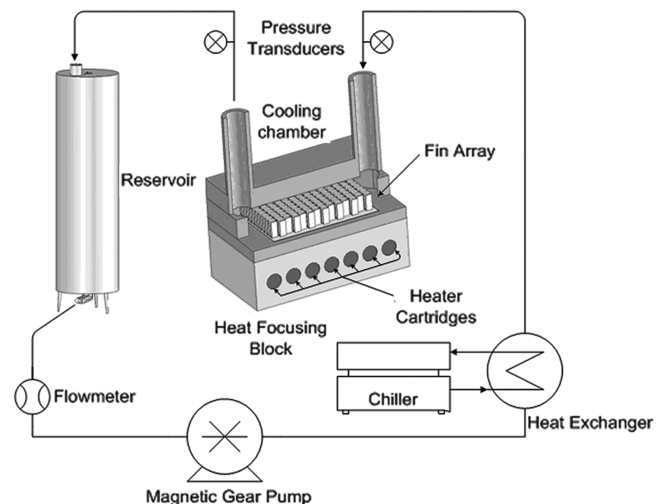


Fig. 1 Schematic of the experimental setup.

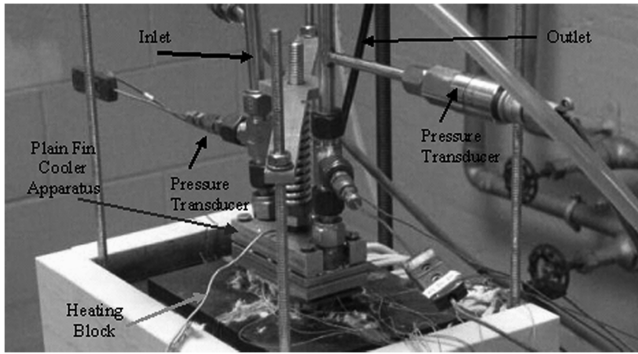


Fig. 2 Photograph of the experimental setup.

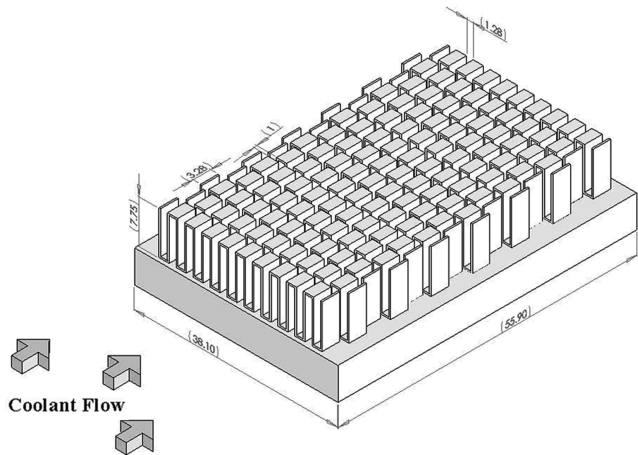


Fig. 3 Schematic of the offset gap plain fin array used in this study.

plate were used to house 10 T-type thermocouples (with a 0.3 mm bead diameter) for measuring the temperature on the bottom of the cooler substrate (Fig. 4). The thermocouples were electrically insulated and mounted in the slots using epoxy glue. Thermal grease (manufactured by Omega) was used to minimize the thermal resistance between the intermediate plate, the heater, and cooler in the sandwich assembly, which was held together by a compression mount. The location of the thermocouples was used to estimate the temperature distribution in the cooler apparatus. The temperatures on the bottom surface were measured by the thermocouples and were used to calculate the surface temperatures at the base of the fins by

$$T_{b,m} = T_{s,m} - (qt_s/k_s) \tag{3}$$

where $T_{b,m}$ is the mean surface temperature at the base of the fin array (top of the base plate), $T_{s,m}$ is the mean surface temperature on the

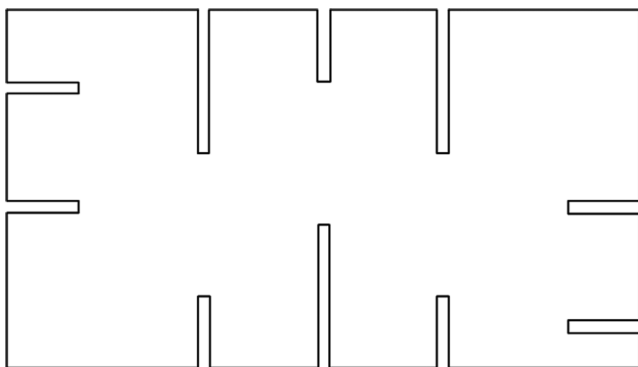


Fig. 4 Layout diagram showing the location of the thermocouples for measuring the temperature at the base of the fin array in the cooler apparatus.

bottom surface of the base plate (measured by the thermocouples shown in Fig. 4), q is the heat flux measured by the thermocouples, t_s is the thickness of the base plate, and k_s is the thermal conductivity of the base plate. Figure 5 shows the layout of the base of the cooler apparatus. In the cooler apparatus, the coolant flowed downward into the cooler, turned 90 deg to the fin channels, crossed the fin array, and then left the cooler at right angles to the substrate. The coolant inlet temperature was maintained at a constant temperature using the heat exchanger apparatus, which was connected to a constant temperature bath. The test fluid inlet and outlet temperatures from the cooler were measured using two thermocouples. The mean temperatures (T_{l-m}) for the test fluids were calculated using the arithmetic mean of the inlet and outlet temperatures of the cooler [26,27]. The test fluid properties were calculated using the mean temperature of the test fluids.

The coolant inlet temperature was held constant at 75°C for these experiments to cross-check the baseline data for a pure solvent, (i.e., PAO) with previous data reported using the same experimental setup [26,27]. The nanofluid used in these experiments were 0.6 and 0.3% by weight of EG in PAO (or 0.5 and 0.25% by volume). During the test, the experimental conditions were varied in the following range: input power, 150–870 W; and coolant flow rate, 0.033–0.078 L/s (0.52–1.25 gpm).

The nanofluids were obtained by dispersing EG nanoparticles (manufactured by the University of Dayton Research Institute) in PAO by using ultrasonication. The nominal particle dimensions designed were 20 μm in diameter and had thicknesses of 100 nm. Figure 6 shows the image of the agglomerated nanoparticles observed under SEM. In this image, the nanoparticles were agglomerated on a copper surface after the PAO solvent was removed using a filter paper. All nanoparticles were functionalized by adding phenyl and carboxylic groups to facilitate their dispersion in the oil. Then the suspension was shear mixed and sonicated for a period of 1 h. Also, the nanofluids were ultrasonicated for 1 h before the start of every experiment or before performing any measurements.

A laser flash apparatus (LFA 447, Netzsch Group, Selb/Bavaria, Germany) was used for thermal diffusivity measurements using a noncontact optical method. A liquid sample is mounted in a transparent cuvette inside the instrument. The cuvette is designed to prevent any bulk convective motion inside the liquid sample. Homogeneous illumination of the entire sample surface is achieved by placing a xenon flash lamp within a parabolic mirror optical-focusing apparatus. The duration and intensity of the light flash can be controlled by instrument software (Naflash software). A liquid-nitrogen-cooled Sb infrared detector is vertically aligned with the light source and the sample holder. The infrared detector is used to measure the temperature rise and time lag after the light pulse. Separate software (called LFA Analysis) is used to calculate the thermal conductivity of the liquid sample based on the transient thermal response of the sample and the characteristics of the incident

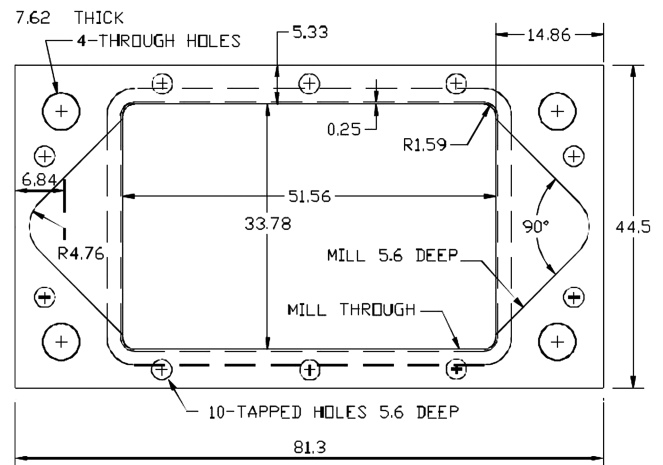


Fig. 5 Layout diagram showing the base of the flow section in the cooler apparatus.

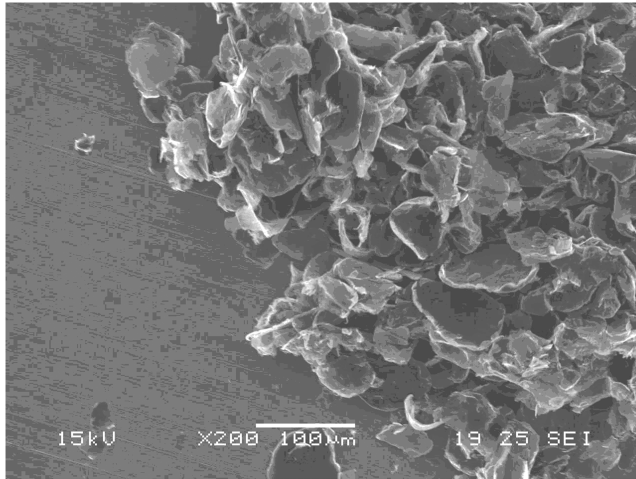


Fig. 6 SEM of the EG nanoparticles. The nanoparticles were obtained after precipitation and agglomeration on a copper surface following the removal of the PAO solvent using filter paper. The nominal sizes of the particles for manufacturing were designed to have a 20 μ diameter and a \sim 100 nm thickness.

light flash. The software has 15 different model options for evaluating the thermal properties of the sample from the raw data using nonlinear regression for different instrument parameters, such as heat loss (from the sides, top, and bottom of sample), with or without pulse length corrections, with or without correlations, etc. Thus, the noncontact mode of measurement obviates the measurement uncertainties for the thermal properties that can be caused by fouling of the sensor elements due to the precipitation of the nanoparticles. A thermocouple inside the sample chamber is used to measure the bulk temperature of the sample. This enables the software to plot the variation of thermal properties with the bulk temperature of the sample. The instrument configuration allows for a short response time that enables rapid data acquisition.

A Hewlett Packard 3852 A data acquisition system was used to record the experimental parameters (the electrical output signals from the measuring instruments for temperature, flow rate, and pressure). The resolution for the temperature measurement for the data acquisition system was 0.02°C and the accuracy of the measured temperature was reported to be 0.2°C [26,27]. The machining and positioning accuracy between any two thermocouples for the heat flux measurement was reported to be 0.3 mm. The uncertainty for the turbine flow meter was 1.9×10^{-3} L/s and for the positive displacement flow meter was 6.3×10^{-4} L/s. After steady-state conditions were reached, all the experimental data (including temperature and flow rates) were acquired 50 times at an interval of 1 min and the average values were recorded. The thermophysical property values for PAO were evaluated at the mean temperature using correlations obtained from the literature [23].

The specific heat was measured by using a differential scanning calorimetry instrument (TA Instruments model Q100). The instrument measurement uncertainty specified by the manufacturer is $\pm 2\%$. The sample was loaded using a cuvette with a sample volume of 100 μ l. The instrument manufacturer specifies the range of the thermal diffusivity measurement for LFA447 to be 0.01–1000 mm²/s with a reproducibility of approximately $\pm 3\%$. Also, a direct determination of the thermal conductivity is possible using this software if the bulk density is known. The software is calibrated against the thermal properties of a known substance.

III. Results and Discussion

Experimental results were obtained for a range of heat fluxes from 3 to 28.5 W/cm² with reference to the heating area (A_h). The property values for PAO were obtained from correlations reported in the literature [23]. The Re was varied from 72 to 365. The heat transfer coefficient was implicitly obtained as follows:

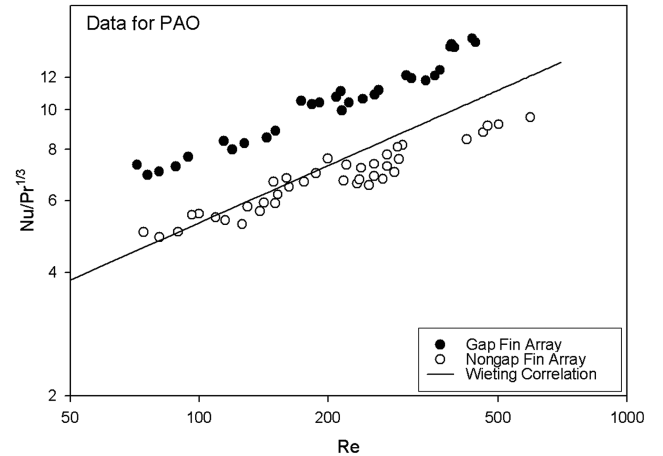


Fig. 7 Performance of the gap fin array (gap = 1 mm) compared with the nongap fin array. The Wieting correlation [32,33] has been plotted for reference.

$$Q = [n_f n_{st} \sqrt{h P k_{fin} A_c} \tanh(sl_1) + A_h h] (T_{b,m} - T_{l,m}) \quad (4)$$

where A_h is the heating area of the base plate not occupied by the fins, $T_{b,m}$ is obtained from Eq. (3), $T_{l,m}$ is the bulk mean temperature of the liquid based on the average of the measured inlet and outlet temperatures, and s is

$$s = \sqrt{\frac{hP}{k_f A_c}} \quad (5)$$

The heat transfer coefficient (h) was iteratively obtained by using Eq. (4) from the experimental data for Q .

A. Baseline Experiments with PAO

The heat transfer data for PAO was expressed by plotting Nu as a function of the of Re and Pr , (i.e., $Nu/Pr^{1/3}$, Fig. 7), which are defined as follows:

$$Re = Ul_1/\nu \quad (6)$$

$$Nu = hl_1/k \quad (7)$$

$$Pr = \nu/\alpha \quad (8)$$

where U is the mass average velocity of the working fluid. The results show that the data for the nongap fins align with the Wieting correlation for Re up to ~ 350 [23,26–29]. Beyond this value of Re , the nongap fin array has a lower Nu than the values predicted by the Wieting correlation, possibly due to variation in pump performance at higher flow rates (e.g., change in pump characteristics). The data for gap fins show an enhancement in the heat transfer coefficient compared with the Wieting correlation. This is consistent with previous observations [26,27] in which the heat transfer coefficient was also reported to be higher for an offset fin strip layout with gaps greater than 1 mm. These experiments were performed to establish the baseline data for comparison with nanofluids. The data also helped to establish any instrument bias compared with previous experiments reported in the literature using the same experimental apparatus [26,27].

B. Thermophysical Property Measurements for PAO Nanofluids

The thermophysical properties that are required to evaluate the forced convective heat transfer performance of nanofluids in these experiments are the specific heat capacity (C_p), density (ρ), viscosity (μ), and thermal conductivity (κ), or thermal diffusivity (α). These properties were needed as a function of the temperature for the temperature range of the experiments (75–140°C) (please see Table A1 in the Appendix).

Specific heat capacity (C_p): The specific heat of the nanofluid and PAO was measured as a function of temperature using differential scanning calorimetry (DSC) and is plotted in Fig. 8. The results show that the specific heat for PAO increases marginally with the temperature. However, there is a marked increase in the specific heat of the nanofluid with the temperature. The specific heat capacity of the nanofluid was found to be enhanced by $\sim 50\%$ compared with PAO at 0.6% concentration by weight.

Based on this single experiment, it is not possible to predict the reason for the unexpected enhancement of specific heat for such minute nanoparticle loading. A potential explanation is based on the expectation that there is a concomitant anomalous increase in the specific heat of the nanoparticles. Wang et al. [30] have shown that the specific heat can be increased substantially by reducing the size and altering the shape of the nanoparticles. The cause of such an anomalous increase was explained by the phonon dispersion (the phonon spectrum changes from continuous to discrete due to the small size of the nanoparticles) and by the softening of atom vibrations that occur due to the interaction of the surface atoms with the interior atoms in the crystal lattice of the nanoparticles (Einstein and Debye vibration modes). Also, other surface phenomena, such as the interaction of the surface atoms of the nanoparticles with the surrounding liquid molecules, can provide additional modes for thermal energy storage (i.e., semisolid behavior) and can play a significant role in increasing the specific heat of the nanofluid. Experimental evidence shows that crystals can induce the ordering of liquid molecules on the surface which, results in a quasi-crystalline structure of the liquid molecules at the surface [31]. Analytical, numerical, and computational models can be developed for explaining the anomalous increase in the specific heat of the nanofluids based on such material behavior. This can be the subject of a future study but is beyond the scope of the current investigation.

Viscosity (μ): The viscosity of the nanofluid (0.6% concentration) was measured using rheometry and was observed to be ~ 10 times higher than PAO (Fig. 9). The rheometry data for nanofluid varied widely for temperatures less than 100°C . The viscosity data for the nanofluid below 100°C have a large spread, and no consistent behavior is discernible. The viscosity of PAO was found to decrease with temperature whereas, for the nanofluid, it was found to increase monotonically with temperature for temperatures exceeding 100°C . A rapid increase in the viscosity of the nanofluid was observed for temperatures greater than 110°C . This shows that the nanofluid may have non-Newtonian behavior at elevated temperatures, possibly leading to the formation of “gel”-type structures that enhance the viscosity. Such a behavior can occur due to the reversible agglomeration of the nanoparticles at elevated temperatures.

Thermal diffusivity (α), density (ρ), and thermal conductivity (κ): These were measured as a function of the temperature for the nanofluid and PAO (Fig. 10). The thermal diffusivity was measured using a laser flash apparatus (LFA 447). It was observed that the

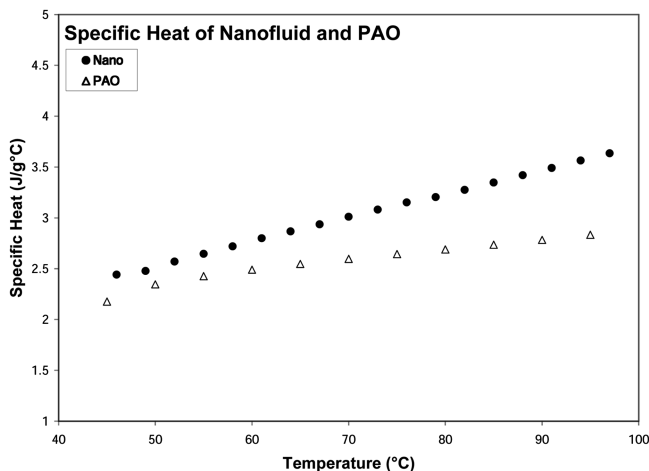


Fig. 8 Variation of the specific heat capacity (C_p in $\text{J/g}^\circ\text{C}$) with the temperature for PAO and the nanofluid with 0.6% EG/PAO by weight.

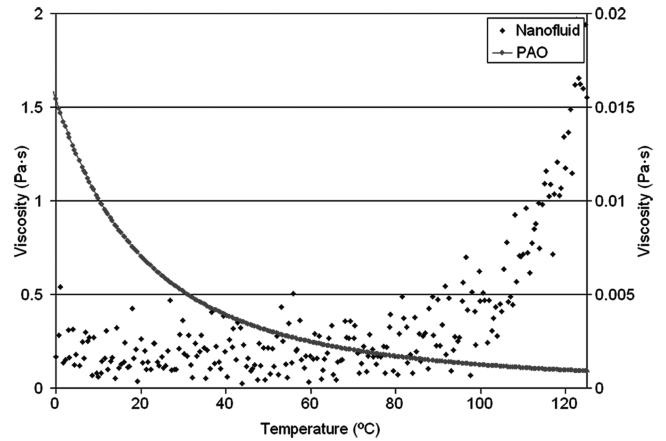


Fig. 9 Viscosity (μ in $\text{Pa}\cdot\text{s}$) as a function of the temperature for the 0.6% EG/PAO nanofluid (primary axis) and PAO (secondary axis) [23].

thermal diffusivity decreased marginally with the temperature for PAO whereas there was a rapid increase in thermal diffusivity of the nanofluid with temperature. Based on the thermal diffusivity of the nanofluid measured experimentally, the thermal conductivity of the nanofluid was calculated to be 4–6 times higher than PAO.

The density of the nanofluid was measured to be 672 kg/m^3 at room temperature ($\sim 300 \text{ K}$). Assuming the density to be constant (in reality, it would potentially decrease marginally with temperature), the thermal conductivity of the nanofluid was compared with that of PAO (Fig. 11). The thermal conductivity of the nanofluid was 10 times higher than that of PAO. The thermal conductivity increased with temperature for the nanofluid and decreased with temperature for PAO. In reality, the density would decrease with temperature. Hence, the trend lines for the thermal conductivity of the nanofluid may have a lower slope in reality than shown in Fig. 11. However, in contrast to the large variation in thermal diffusivity ($\sim 400\%$), a marginal variation in density can be expected for the nanofluid (expected to be less than 10%). Similarly, the variation in viscosity for the nanofluid is substantially larger than can be expected for the variation of the density. Hence, the effect of the density variation on the thermal conductivity data (or Reynolds number values) is expected to be marginal.

C. Flow-Loop Experimental Results

The flow-loop experiments were conducted by parametrically increasing the heat input from the cartridge heaters for a given flow rate. Experiments were also conducted by parametrically varying the flow rates. The results from these experiments are plotted for different values of heat input to the cartridge heaters (Figs. 12–14). The results show that the heat flux increases with flow rate for both

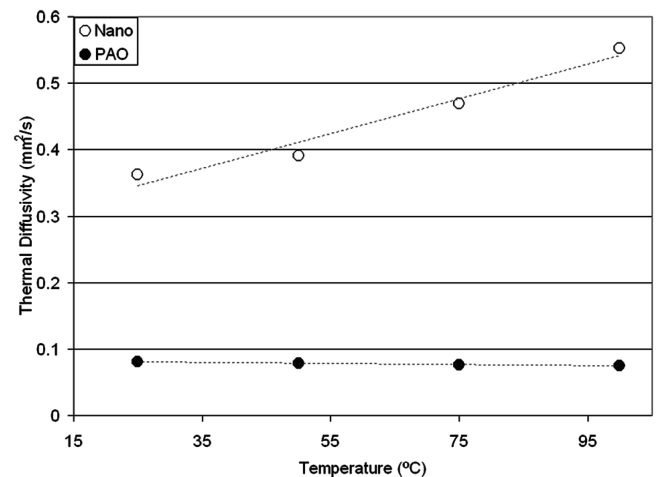


Fig. 10 Variation of the thermal diffusivity (α in mm^2/s) with the temperature for the 0.6% EG/PAO nanofluid and PAO [23].

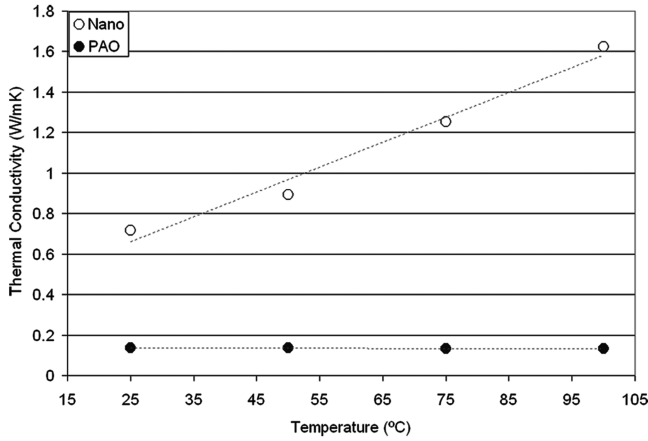


Fig. 11 Variation of the thermal conductivity (κ in $W/m\ ^\circ C$) with the temperature for the 0.6% EG/PAO nanofluid and PAO. The density (ρ) of nanofluid is assumed to be constant at a room temperature value of $672\text{ kg}/m^3$.

fluids. It was also observed that there is a consistent 8–10% enhancement in heat flux for nanofluids compared with PAO for a given flow rate.

At a heat input of 300 W to the cooler, it was observed that the heat flux in the cooler increased with the flow rate. The heat flux was enhanced by ~3% at a flow rate of 0.013 L/s and by ~5% at a flow rate of 0.079 L/s for the nanofluid (0.3% EG/PAO by weight) compared with pure PAO. The heat flux was enhanced by ~5% at a flow rate of 0.013 L/s and by ~7% at a flow rate of 0.079 L/s for the nanofluid (0.6% EG/PAO by weight) compared with pure PAO. It was observed that the rate of heat flux increase with the flow rate was higher for both types of nanofluid than for pure PAO.

At a heat input of 400 W to the cooler, it was observed that the heat flux in the cooler increased with the flow rate. The heat flux was enhanced by ~3% at a flow rate of 0.013 L/s and by ~4% at a flow rate of 0.079 L/s for the nanofluid (0.3% EG/PAO by weight) compared with pure PAO. The heat flux was enhanced by ~8% at a flow rate of 0.013 L/s and by ~10% at a flow rate of 0.079 L/s for the nanofluid (0.6% EG/PAO by weight) compared with pure PAO. It was observed that the rate of heat flux increase with the flow rate was higher for both types of nanofluid than for pure PAO.

At a heat input of 500 W to the cooler, a peculiar behavior was observed for the cooling capacity of the nanofluid. It was observed for the 0.6% EG/PAO nanofluid that, initially, the heat flux in the cooler increased rapidly with the flow rate, following which the heat flux marginally increased and attained a constant value of $27.3\text{ W}/cm^2$. For the 0.3% EG/PAO nanofluid, it was observed that there was no heat transfer enhancement for flow rates below 0.063 L/s. For flow rates exceeding 0.063 L/s, the heat flux in the

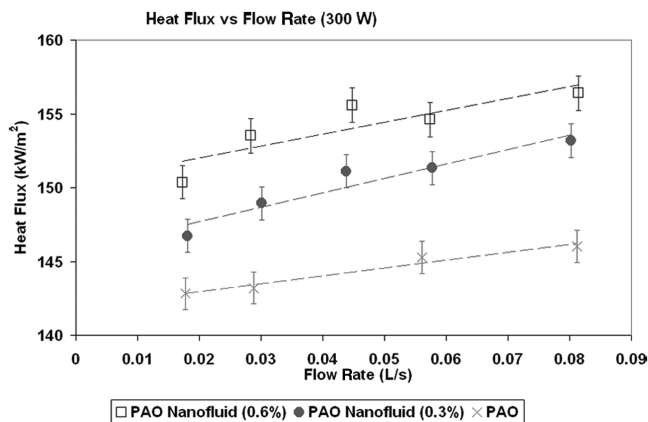


Fig. 12 Variation of the heat flux (kW/m^2) with the flow rate (gpm) for a heat input of 300 W.

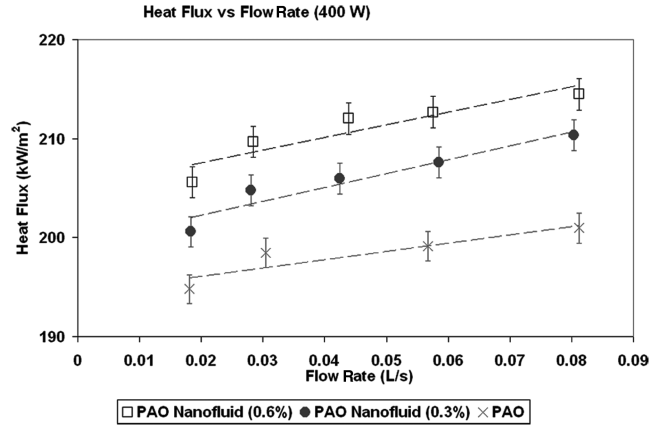


Fig. 13 Variation of the heat flux (kW/m^2) with the flow rate (gpm) for a heat input of 400 W.

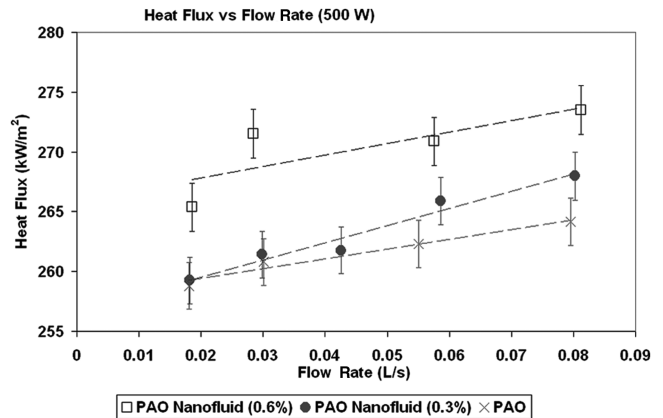


Fig. 14 Variation of the heat flux (kW/m^2) with the flow rate (gpm) for a heat input of 500 W.

nanofluid was enhanced by ~2% for flow rates of 0.063 and 0.079 L/s. It is possible that at elevated heat fluxes the surface temperature of the offset gap fin array exceeded $110^\circ C$, causing the agglomeration of the nanoparticles and hence reducing their ability to transport heat in forced convection. It should be noted that a small dip in the heat flux data is observed in Figs. 12–14 at the flow rate of 0.057 L/s. A different gear pump was used for flow rates exceeding 0.05 L/s. This would explain that the dip in the data is possibly due to a change in pump characteristics.

To evaluate the efficacy of the nanofluids for convective heat transfer, their performance was evaluated using nondimensional parameters. For example, Nu was plotted as a function of Re and Pr (for both PAO and the nanofluid, Figs. 15–17) for different power input conditions. Because the viscosity of the nanofluid is ~10 times higher, the Re for the same flow rate is therefore lower compared with the Re for PAO. Hence, the data for the two fluids do not overlap for a given Re . The graphs show that same value of Nu is obtained at a much lower value of $(RePr^{1/3})$. This shows that the nanofluid has better heat transfer characteristics for a given Re . Also, in Fig. 17, marginally higher values of Nu are observed for the same Re for the nanofluid at power input conditions of 500 W than for the input conditions of the 300 and 400 W cases. This is possibly due to the higher viscosity of the nanofluid caused by the higher average operating temperature of the bulk fluid at 500 W. By Reynolds analogy, the higher viscosity would cause a higher pressure drop which in turn could lead to an enhancement of Nu .

Figure 18 shows the representative surface temperature distribution at the bottom of the fin array plotted based on temperature measurements at four different locations on the base plate. The direction of the flow inlet and outlet is indicated by an arrow in the figure. The locations of the four thermocouples used for the measurements are plotted on the x and y axes and are marked as east,

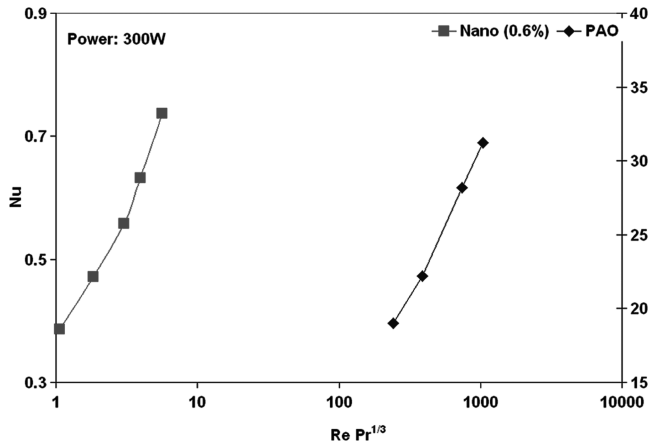


Fig. 15 Comparison of Nu as a function of $(RePr^{1/3})$ at power input = 300 W for the PAO nanofluid (0.6% concentration) and PAO.

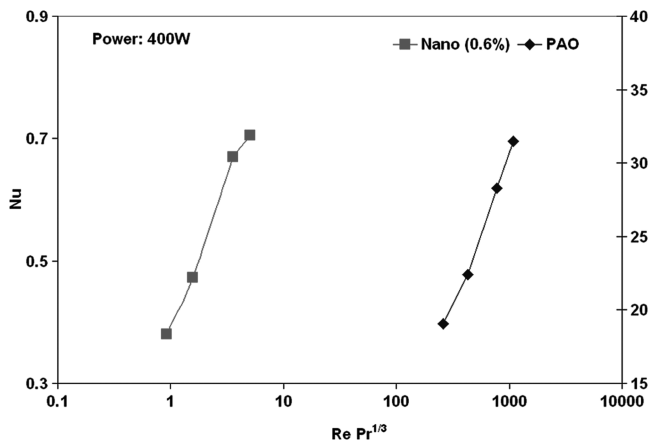


Fig. 16 Comparison of Nu as a function of $(RePr^{1/3})$ at power input = 400 W for the PAO nanofluid (0.6% concentration) and PAO.

west, north, and south. The temperature values are plotted on the z axis at each of these locations, and the 3-D plot of the surface representing the temperature profile is obtained. The interpolated values of the temperature are also shown on the plotted surface. The figure shows that the temperature rises from the inlet (marked as east) until just before the outlet (marked as west). Similar plots are obtained for other flow rate and heat flux values. The calculations outlined in Eqs. (3–5) are performed by taking the average of the surface temperature values shown in Fig. 18.

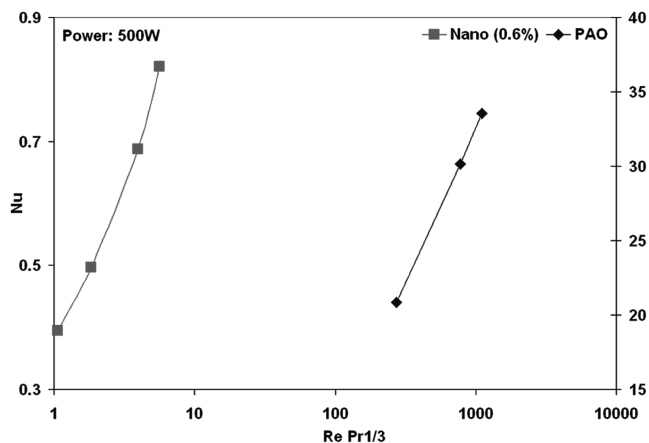


Fig. 17 Comparison of Nu as a function of $(RePr^{1/3})$ at power input = 500 W for the PAO nanofluid (0.6% concentration) and PAO.

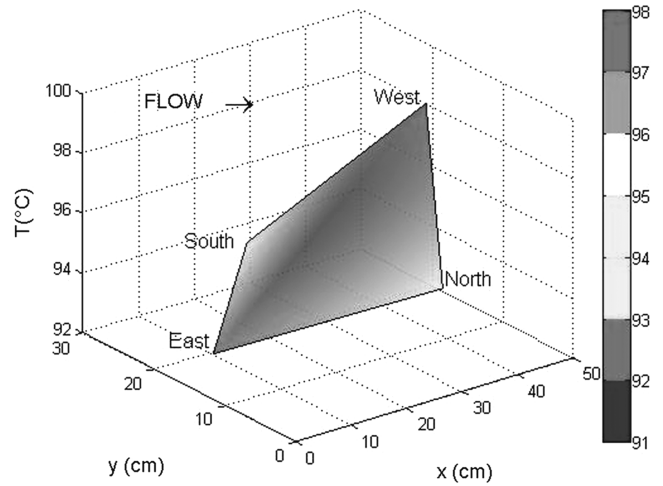


Fig. 18 Plot of the representative temperature distribution on the bottom of the base plate for a flow rate of 0.057 L/s and heat input of 300 W.

D. Scanning Electron Micrography and Energy Dispersive X-Ray Spectra

To explore the reason behind the enhancement of heat flux for nanofluids, it was hypothesized that the nanofluids deposit nanoparticles on the walls of the cooler (possibly due to electrostatic interactions). These nanoparticles act as nanofins, which enhance the effective surface area of the walls and therefore act as enhanced heat transfer surfaces. To test this hypothesis, a fin surface was observed under microscope and EDX analyses for the composition of the precipitated nanoparticles were performed. Figure 19 shows a representative SEM of the fin surface. The deposited nanoparticles appear as semitransparent polygons because they are transparent to the electron source owing to their thin lamellar structure. The composition of the deposited nanoparticles was analyzed by EDX spectra (Fig. 20). Sharp peaks for carbon were observed in the spectra and marginal peaks were observed for copper. The spectra show that the majority of the deposited particles are from carbon. Hence, the EDX spectra confirm the nanoscale deposition of carbon material on the copper surface, which potentially occurs from the deposition of the exfoliated graphite nanoparticles.

As shown in Ding et al. [24], the lower aspect ratio of graphite nanoparticles limit the heat transfer enhancement of nanofluids. In contrast, the higher aspect ratio of carbon nanotubes results in a higher enhancement of thermal conductivity as well as forced convective heat transfer.

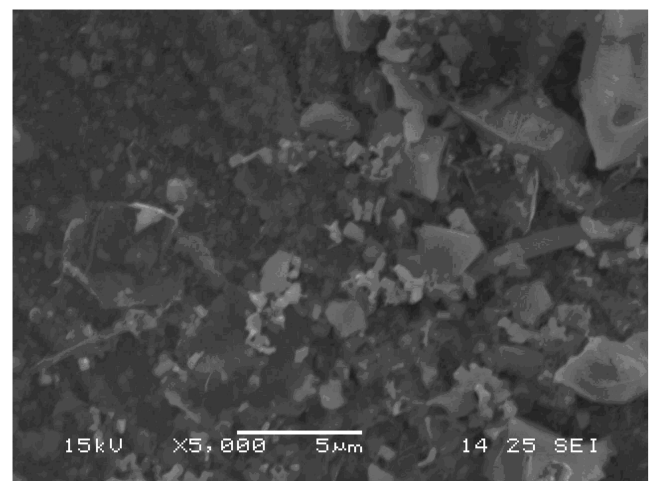


Fig. 19 SEM of nanoparticles deposited on the fin surface showing the formation of nanofins that effectively serve as enhanced heat transfer surfaces.

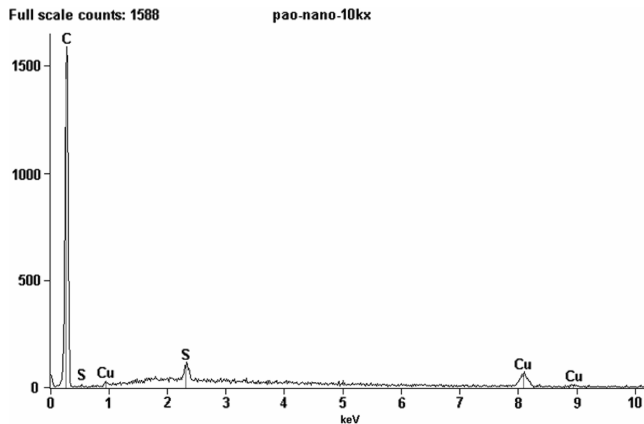


Fig. 20 EDX spectra for deposits on the plain fin surface in the cooler apparatus. The spectra show the deposition of carbon material on copper surface.

IV. Conclusions

The experiments were conducted using PAO and nanofluids. The baseline performance was established using PAO and compared with the Wieting correlation. This was followed by a comparison with the thermal performance of the nanofluids. The nanofluids were found to enhance the heat flux in a flow loop containing a cooler with offset gap fins. The nanofluids were also found to have enhanced thermophysical properties (viscosity, specific heat capacity, thermal conductivity, and diffusivity). Analyses of the nondimensional parameters (i.e., Nu vs Re and Pr) show that a substantial enhancement in Nu is obtained for lower Re for the nanofluids when compared with PAO. The plausible reason for the heat transfer enhancement is due to the precipitation of the nanoparticles that occurs, especially at low particle loading. This surface precipitates can interact with the fluid and alter the flow conditions. It can also lead to an enhanced surface area at the wall. SEM and EDX measurements confirm that the nanofluids deposit nanoparticles on the surface that act as enhanced heat transfer surfaces (nanofins). At a higher particle loading of the nanoparticle, such precipitation can cause a fouling of the heat transfer surface and degrade the thermal performance of the nanofluids.

Appendix

Table A1 Thermophysical properties of PAO and nanofluids

Property data, 75°C	PAO	PAO nanofluid: EG of 0.6% by weight in PAO
Density, kg/m ³	749	762
Viscosity, Pa · s	0.00183	0.02–0.5
Specific heat, kJ/°C kg	2.33	3.12
Thermal diffusivity, mm ² /s	0.076	0.469

Acknowledgments

Debjyoti Banerjee thanks the U.S. Air Force Office of Scientific Research (AFOSR) and the American Society for Engineering Education (ASEE) for providing the U.S. Air Force Research Laboratory (AFRL) Summer Faculty Fellowship (2006) that enabled this study. Ian C. Nelson thanks the AFOSR and Universal Energy Systems (UES) for the summer financial support that enabled participation in this research work. The authors would like to express their sincere gratitude to L. Lin (University of Dayton Research Institute, or UDRI), Dick Harris (UDRI), Roger Carr (UDRI), Jacob Lawson (UDRI), and John Tennant (UES) for their help with performing the experiments. The authors also thank Sabyasachi (Raj) Ganguli (contractor/AFRL) and Ajit Roy (Materials Directorate/AFRL) for their help with the thermophysical measure-

ments (specific heat). The assistance of S. Ganguly, U.S. Air Force Research Laboratory/Materials Directorate, in obtaining the measurements used in Fig. 8 is duly acknowledged. Last but not least, the authors thank K. Lafdi (UDRI) for his help with preparing the nanofluids and for the thermophysical measurement data for the nanofluids.

References

- [1] Lee, S., Choi, S. U.-S., Li, S., and Eastman, J. A., "Measuring Thermal Conductivity of Fluids Containing Oxide Nanoparticles," *Journal of Heat Transfer*, Vol. 121, No. 2, May 1999, pp. 280–289. doi:10.1115/1.2825978
- [2] Koblinski, P., Eastman, J. A., and Cahill, D. G., "Nanofluids for Thermal Transport," *Materials Today*, Vol. 8, No. 6, June 2005, pp. 36–44. doi:10.1016/S1369-7021(05)70936-6
- [3] Wang, X.-Q., and Mujumdar, A. S., "Heat Transfer Characteristics of Nanofluids: A Review," *International Journal of Thermal Sciences*, Vol. 46, No. 1, Jan. 2007, pp. 1–19. doi:10.1016/j.ijthermalsci.2006.06.010
- [4] Maxwell, J. C., *A Treatise on Electricity and Magnetism*, 2nd ed., Clarendon, Oxford, 1881.
- [5] Hamilton, R. L., and Crosser, O. K., "Thermal Conductivity of Heterogeneous Two-Component Systems," *Industrial & Engineering Chemistry Fundamentals*, Vol. 1, 1962, pp. 182–191.
- [6] Prasher, R., Bhattacharyya, P., and Phelan, P. E., "Brownian-Motion-Based Convective-Conductive Model for Effective Thermal Conductivity of Nanofluids," *Journal of Heat Transfer*, Vol. 128, No. 6, June 2006, pp. 588–595. doi:10.1115/1.2188509
- [7] Putnam, S. A., Cahill, D. G., Braun, P. V., Ge, Z., and Shimmin, G., "Thermal Conductivity of Nanofluid Suspension," *Journal of Applied Physics*, Vol. 99, No. 8, 2006, Paper 084308.
- [8] You, S. M., and Kim, J. H., "Effect of Nanoparticles on Critical Heat Flux of Water in Pool Boiling Heat Transfer," *Applied Physics Letters*, Vol. 83, No. 16, Oct. 2003, pp. 3374–3376.
- [9] Vassallo, P., Kumar, R., and Amico, S. D., "Pool Boiling Heat Transfer Experiments in Silica-Water Nanofluids," *International Journal of Heat and Mass Transfer*, Vol. 47, No. 2, 2005, pp. 407–411.
- [10] Das, S. K., Putra, N., and Roetzel, W., "Pool Boiling Characteristics of Nanofluids," *International Journal of Heat and Mass Transfer*, Vol. 46, No. 5, 2003, pp. 851–862.
- [11] Das, S. K., Putra, N., and Roetzel, W., "Pool Boiling of Nanofluids on Horizontal Narrow Tubes," *International Journal of Multiphase Flow*, Vol. 29, No. 8, 2003, pp. 1237–1247.
- [12] Li, C. H., Wang, B. X., Peng, X. F., "Experimental Investigations on Boiling of Nano-Particle Suspensions," *Proceedings of the Boiling Heat Transfer Conference*, James Klausner, Gainesville, FL, 2003.
- [13] Wasan, D. T., and Nikolov, A. D., "Spreading of Nanofluids on Solids," *Nature (London)*, Vol. 423, May 2003, pp. 156–159.
- [14] Guinn, J., and Banerjee, D., "Experimental Study of Nanofluids for Droplet Cooling Applications Using Temperature Micro-Sensors," American Society of Mechanical Engineers Paper 2006-14101, 2006.
- [15] Jackson, J. E., Borgmeyer, B. V., Wilson, C., Cheng, P., and Bryan, J. E., "Characteristics of Nucleate Boiling with Gold Nanoparticles in Water," American Society of Mechanical Engineers Paper 2006-16020, 2006.
- [16] Mills, A. F., *Heat and Mass Transfer*, Irwin Publishers, Boston, 1995.
- [17] Pak, B. C., and Cho, Y. I., "Hydrodynamic and Heat Transfer Study of Dispersed Fluids with Sub-Micron Metallic Oxide Particles," *Experimental Heat Transfer*, Vol. 11, No. 2, 1998, pp. 151–170.
- [18] Xuan, Y., and Li, Q., "Investigation of Convective Heat Transfer and Flow Features of Nanofluids," *Journal of Heat Transfer*, Vol. 125, Feb. 2003, pp. 151–155.
- [19] Eastman, J. A., Choi, U. S., Li, S., Soye, G., Thompson, L. J., and DiMelfi, R. J., "Novel Thermal Properties of Nanostructured Materials," *Materials Science Forum*, Vols. 312–314, 1999, pp. 629–634.
- [20] Wen, D., and Ding, Y., "Experimental Investigation into Convection Heat Transfer of Nanofluids at the Entrance Region Under Laminar Flow Conditions," *International Journal of Heat and Mass Transfer*, Vol. 47, No. 24, Nov. 2004, pp. 5181–5188. doi:10.1016/j.ijheatmasstransfer.2004.07.012
- [21] Yang, Y., Zhang, Z. G., Grulke, E. A., Anderson, W. B., and Wu, G., "Heat Transfer Properties of Nanoparticle-in-Fluid Dispersions (Nanofluid) in Laminar Flow," *International Journal of Heat and Mass Transfer*, Vol. 48, No. 6, March 2005, pp. 1107–1116. doi:10.1016/j.ijheatmasstransfer.2004.09.038

- [22] Heris, S. Z., Etemad, S. G., and Esfahany, M. N., "Experimental Investigation of Oxide Nanofluids Laminar Flow Convective Heat Transfer," *International Communications in Heat and Mass Transfer*, Vol. 33, No. 4, April 2006, pp. 529–535.
doi:10.1016/j.icheatmasstransfer.2006.01.005
- [23] Ghajar, A. J., Tang, W. C., and Beam, J. E., "Comparison of Hydraulic and Thermal Performance of PAO and Coolanol 25R Liquid Coolants," AIAA Paper 1994-1965, 1994.
- [24] Ding, Y., Alias, H., Wen, D., and Williams, R. A., "Heat Transfer of aqueous suspensions of carbon nanotubes (CNT nanofluids)," *International Journal of Heat and Mass Transfer*, Vol. 49, Nos. 1–2, Jan. 2006, pp. 240–250.
doi:10.1016/j.ijheatmasstransfer.2005.07.009
- [25] Sieder, E. N., and Tate, G. E., "Heat Transfer and Pressure Drop of Liquids in Tubes," *Industrial and Engineering Chemistry*, Vol. 28, No. 12, 1936, pp. 1429–1435.
doi:10.1021/ie50324a027
- [26] Lin, L., "Thermal Management Research for Power Generation," U.S. Air Force Research Laboratory, AFRL-PR-WP-TR-2003-2051, Wright-Patterson Air Force Base, Dec. 2002.
- [27] Lin, L., Ponnappan, R., and Leland, J. E., "Heat Transfer Correlations for Plain Fin Array Cooler," AIAA Paper 2002-0207, 2002.
- [28] Wieting, A. R., "Empirical Correlations for Heat Transfer and Flow Friction Characteristics of Rectangular Offset-Fin Plate-Fin Heat Exchangers," *Journal of Heat Transfer*, Vol. 97, Aug. 1975, pp. 488–490.
- [29] Joshi, H. M., and Webb, R. L., "Heat Transfer and Friction in the Offset Strip-Fin Heat Exchanger," *International Journal of Heat and Mass Transfer*, Vol. 30, No. 1, Jan. 1987, pp. 69–84.
doi:10.1016/0017-9310(87)90061-5
- [30] Wang, B-X., Zhou, L-P., and Peng, X-F., "Surface and Size Effects on the Specific Heat Capacity of the Nanoparticles," *International Journal of Thermophysics*, Vol. 27, No. 1, Jan. 2006, pp. 139–151.
doi:10.1007/s10765-006-0022-9
- [31] Oh, S. H., Kauffman, Y., Scheu, C., Kaplan, W. D., and Ruhle, M., "Ordered Liquid Aluminum at the Interface with Sapphire," *Science*, Vol. 310, No. 5748, Oct. 2005, pp. 661–663.
doi:10.1126/science.1118611
- [32] Wieting, A. R., "Empirical Correlations for Heat Transfer and Flow Friction Characteristics of Rectangular Offset-Fin Plate-Fin Heat Exchangers," *Journal of Heat Transfer*, Vol. 97, Aug. 1975, pp. 488–490.
- [33] Joshi, H. M., and Webb, R. L., "Heat Transfer and Friction in the Offset Strip-Fin Heat Exchanger," *International Journal of Heat and Mass Transfer*, Vol. 30, No. 1, 1987, pp. 69–84.
doi:10.1016/0017-9310(87)90061-5